Spectroscopic properties and singlet oxygen production by the compound ethyl 3,12-dioxopyran[3,2-a]xanthone-2-carboxylate

ARTICLE *in* SPECTROCHIMICA ACTA PART A MOLECULAR AND BIOMOLECULAR SPECTROSCOPY · JULY 2013

Impact Factor: 2.35 · DOI: 10.1016/j.saa.2013.06.087 · Source: PubMed

Spectrochimica Acta Part A: Molecular and Biomolecular Spectroscopy 115 (2013) 610–616

Contents lists available at SciVerse ScienceDirect

Spectrochimica Acta Part A: Molecular and Biomolecular Spectroscopy

journal homepage: www.elsevier.com/locate/saa

Spectroscopic properties and singlet oxygen production by the compound ethyl 3,12-dioxopyran[3,2-a]xanthone-2-carboxylate

Antonio Eduardo da Hora Machado [a,b,*], Lucas Ferreira de Paula [a], Ana Maria Ferreira de Oliveira-Campos [c], Anderson de Jesus Gomes [d], Rodrigo de Paula [e], Newton Martins Barbosa Neto [a,f]

[a] Universidade Federal de Uberlândia, Instituto de Química, Laboratório de Fotoquímica e Ciência de Materiais, P.O. Box 593, CEP 38400-902, Uberlândia, Minas Gerais, Brazil
[b] Universidade Federal de Goiás, Campus Catalão, Departamento de Química, Catalão, Goiás, Brazil
[c] Universidade do Minho, Centro de Química, Campus de Gualtar, Braga, Portugal
[d] Universidade de Brasília, Faculdade Ceilândia, Brasília, Brazil
[e] Universidade Federal do Recôncavo da Bahia, Centro de Formação de Professores Amargosa, Bahia, Brazil
[f] Universidade Federal de Uberlândia, Instituto de Física, Uberlândia, Minas Gerais, Brazil

HIGHLIGHTS

- The compound ethyl 3,12-dioxopyran[3,2-a]xanthone-2-carboxylate was studied.
- This study involved experimental measurements and quantum-mechanical calculations.
- Spectroscopic and quantum-mechanical data agree very well.
- High efficiency in the generation of singlet oxygen.
- This compound can be a promising phototherapeutic agent for PUVA therapy.

GRAPHICAL ABSTRACT

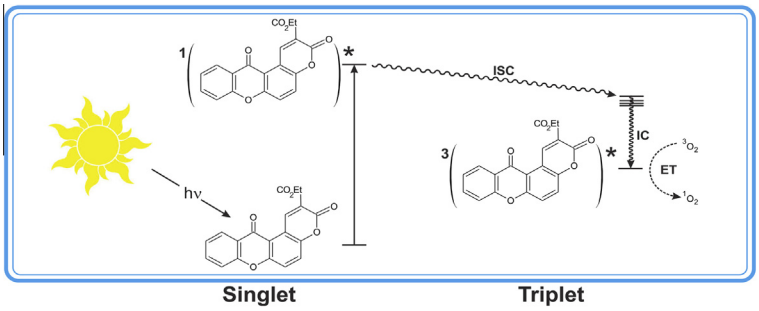

ARTICLE INFO

Article history:
Received 6 April 2013
Received in revised form 18 June 2013
Accepted 24 June 2013
Available online 3 July 2013

Keywords:
Xanthone
Absorption
Emission
DFT and TD-DFT
Singlet oxygen
PUVA therapy

ABSTRACT

The steady state and time resolved experiments together with absorption and emission spectroscopies and quantum chemical calculations have been employed to investigate spectroscopic properties of a xanthone-type compound (ethyl 3,12-dioxopyran[3,2-a]xanthone-2-carboxylate). The spectroscopic data show good agreement with results obtained from quantum chemical calculations. Additionally, this compound shows expressive quantum efficiency for triplet population and a quantum efficiency of singlet oxygen generation very close to unity. Correlations between the nature of singlet and triplet excited states and spectroscopic properties were performed in order to understand the high quantum efficiency of singlet oxygen generation by this compound.

Introduction

Some natural psoralens have been used as photosensitizing drugs in PUVA (Psoralen and UVA light) therapy, a therapeutic combination of psoralens and UVA (ultraviolet radiation in the range between 400 and 315 nm) light [1–10]. However, PUVA ther-

* Corresponding author at: Universidade Federal de Uberlândia, Instituto de Química, Laboratório de Fotoquímica e Ciência de Materiais, P.O. Box 593, CEP 38400-902, Uberlândia, Minas Gerais, Brazil. Tel.: +55 34 3239 4428; fax: +55 34 3239 4208.
E-mail address: aehmachado@gmail.com (A.E. da Hora Machado).

1386-1425/$ - see front matter © 2013 Elsevier B.V. All rights reserved.
http://dx.doi.org/10.1016/j.saa.2013.06.087

apy using natural psoralens tends to present health risks [9–12]. The action of naturally occurring psoralens in PUVA therapy is related to the ability of these compounds to cause DNA damage: in the absence of light, these compounds tend to interleave the base pairs of the DNA forming weak molecular complexes, without significant biological effects [1,11–14]. When exposed to UVA radiation, these complexes react with pyrimidine bases of DNA, resulting in covalent mono-and bifunctional cycloadducts, a risk factor of mutagenicity and its consequences, such as both nonmelanoma skin cancer and melanoma [10–14].

It is known that some psoralen analogues based on dibenzofuran (benzopsoralens) are capable to sensitize singlet oxygen with high quantum efficiency [15,16], which, given the cytotoxicity of this species, makes them interesting for application in PUVA therapy [17,18]. The presence, in certain synthetic benzopsoralens, of substituents at positions more labile for intercalation to DNA, hindering or even preventing the formation of derivatives, results in favorable consequences for the application of PUVA therapy [1], since it should result in lower health risks for the patient. These compounds have shown biological activity, with a good ability to inhibit *in vitro* growth of strains of malignant tumor in the absence of light [15,19]. In addition to the cytotoxic effects in the absence of light, some of these compounds when irradiated induce phototoxic effects such as swelling of the nuclear membrane, mitochondrial damage, and cytoplasmic vesiculation [20–24].

It is also known that xanthones tend to present a high efficiency of triplet population, assigned to $^1\pi\pi^* \rightarrow {}^3n\pi^*$ transitions [25]. In the present study a benzopsoralen analogue, ethyl 3,12-dioxopyran[3,2-a]xanthone-2-carboxylate (PXO1), formed by the condensation of a pyranone to a xanthone ring, see Fig. 1, was investigated. Its synthesis was previously described [26].

Such compound has shown a dark growth pronounced inhibitory effect against MCF-7, SF-268 and NCI-H460 cell lines [26]. Apparently the biological activity is correlated to the arrangement of the rings in the plane of the molecule [19,26], a characteristic also reported for benzopsoralens capable to sensitize the generation of singlet oxygen [16]. In order to contribute to the understanding of the origin of so promising photobiological features, the photophysics and spectroscopic properties were investigated using absorption and emission spectroscopic techniques in association with quantum chemical calculations. Its capability to sensitize the generation of singlet oxygen using time resolved and steady-state methodologies were also evaluated.

Experimental and theoretical methods

Spectroscopic measurements

The absorption spectrum was obtained from a solution prepared in methanol. Luminescence measurements were performed at 298 K and 77 K using anhydrous ethanol as solvent, being the emission and excitation slits of 2.5 nm, using a xenon lamp. The PMT was operated at 950 V, and the scanning rate was set to 240 nm min^{-1}. Argon was used to deoxygenate the solutions, previously to experiments when needed. All solvents used were of spectroscopic grade.

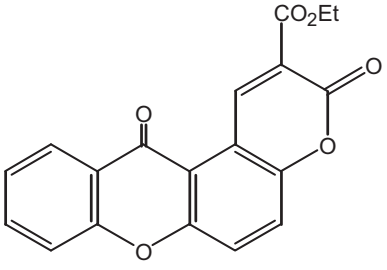

Fig. 1. Representation of the compound ethyl 3,12-dioxopyran[3,2-a]xanthone-2-carboxylate, PXO1.

UV/VIS absorption and emission spectra were recorded respectively using a Shimadzu UV-1650PC spectrophotometer and a HITACHI F-4500 spectrofluorimeter equipped with accessories for low temperature measurements, being the fluorescence spectra obtained using right angle configuration. The low lying electronic absorption maxima were used as excitation wavelength for all samples. The absorbance at this wavelength was maintained below 0.100 to avoid light reabsorption effects [27].

The fluorescence quantum yield was estimated from the corrected fluorescence spectra, using the secondary standard methodology [28]. The compound 9,10-diphenylantracene in cyclohexane (Φ_F = 0.90 at 293 K) was used as fluorescence standard.

Quantum yield of singlet oxygen generation

The quantum yield of singlet oxygen generation, Φ_Δ, was estimated by steady-state and time-resolved measurements. The steady-state measurements were based on the monitoring of consumption of 1,3-diphenylisobenzofuran (DPBF),

$$\Phi_\Delta = \frac{k_r}{I_a}\frac{(I_a\Phi_\Delta)_S}{(k_r)_S} \quad (1)$$

The parameters I_a and $I_{a,S}$, respectively the emission intensity of the sample and the emission intensity of the standard, were quantified using a Solar Light PMA 2100 version 1.17 radiometer, equipped with an UVA detector.

The rates $(k_r)_S$ and k_r, respectively of consumption of DPBF (measured at 417 nm) by the singlet oxygen produced by photosensitization by the standard 1-perinaphthenone [29], and by the PXO1, both in methanol, were estimated considering that the reaction between singlet oxygen and DPBF follows a pseudo-first order kinetics under the present conditions [30]. The rates $(k_r)_S$ and k_r were corrected subtracting the DPBF degradation rate occurred by direct photolysis. The Φ_Δ estimated for 1-perinaphthenone in methanol [29] was used as standard ($\Phi_{\Delta,S}$) for these measurements.

For the time-resolved measurements, a LP 900 Edinburgh Analytical Instruments time-resolved system was used. In such system, a Nd-YAG CONTINUUM SURELITE II (Q-switched delay 200 μs) laser providing 5 ns laser pulses (5 mJ/pulse) at 355 nm was employed as excitation source, and a Hamamatsu R-5509 photomultiplier, cooled at 193 K was used for the detection of singlet oxygen phosphorescence at 1270 nm. The absorbance of the solutions was adjusted to 0.300 at 355 nm. In these measurements, the right-angle configuration was used for all samples and standard. The equation,

$$\Phi_{\Delta,a} = \frac{I_a}{I_s}\Phi_{\Delta,s} \quad (2)$$

was used to calculate Φ_Δ. I_a is the initial emission intensity of the sample at 1270 nm, and I_s the emission intensity of the standard 1-perinaphthenone [29] under the same conditions. $\Phi_{\Delta,a}$ is the quantum efficiency of singlet oxygen generation by the sample. Methanol was used as solvent in these measurements.

Triplet lifetime

PXO1 triplet lifetime was evaluated using a flash photolysis system and previously deaerated (argon) solutions prepared in methanol, containing the compound under investigation. The

samples were excited with an Nd-YAG CONTINUUM SURELITE II (Q-switched delay 200 μs) laser at 355 nm. All decays were monitored at 600 nm – absorption maximum estimated from transient spectrum of triplet in the range between 360 and 700 nm. The laser flash photolysis decay profiles were captured using a Hewlett–Packard model 54510B digitizing oscilloscope interfaced to a PC.

Computational details

The singlet ground state structure of PXO1 was optimized under two conditions: (a) using directly the structure of the compounds in a SCRF calculation based on the application of the model IEFPCM [31,32] to build a continuum of uniform dielectric constant corresponding to methanol, and (b) PXO1 involved by a finite number of explicit molecules of methanol in a SCRF calculation based on the application of the model IEFPCM to build a continuum of uniform dielectric constant corresponding to methanol. In both situations the 6-311G(d,p) basis set and the B3LYP hybrid functional [33] were used. All calculations were done without any symmetry constraints, and geometries were confirmed as stationary structures by the presence of only real frequencies at the same level of theory.

The lowest 25 singlet-singlet and 6 singlet-triplet excitations and the corresponding oscillator strengths were calculated from the optimized structures using the B3LYP hybrid functional in a TD-DFT approach, using the 6-311++G(2d,2p) basis set and the IEFPCM model. The singlet-singlet excitation spectrum and the energy diagram for the first non-relaxed states were built from these data. A state diagram for the first relaxed excited states was also built. The energies were calculated using TD-DFT after geometry optimization of the excited states using *ab initio* calculation at the CIS level [34], in order to match the energies with the obtained in the calculations of electronic excitation. These calculations were done using the 6-31G(d,p) basis set.

All calculations were done using Gaussian 09 [35] and GaussView 5.0.8 [36] was employed in the analysis of the results.

Results and discussion

Theoretical simulations

In order to minimize the limitations of continuum dielectric models in the description of specific solute-solvent interactions, such as hydrogen bonds, we use the combination of a set of explicit solvent molecules, arranged around the species under study, with the IEFPCM model, to represent the solvation. The explicit solvent molecules were positioned aiming to establish hydrogen bonds with each other and with the PXO1. The positions of interaction were chosen considering the Mulliken atomic charge distribution for the optimized PXO1, employing only the dielectric continuum model. Fig. 2 shows the model containing explicit methanol molecules plus PXO1, enveloped by a continuum of uniform dielectric constant corresponding to methanol, generated by the IEFPCM model.

Electronic absorption spectrum

The electronic absorption spectrum of PXO1 in methanol, Fig. 3, exhibits maxima at 244 nm (A; $\varepsilon = 38{,}670\ L\ mol^{-1}\ cm^{-1}$), 300 nm (B; $\varepsilon = 16{,}226\ L\ mol^{-1}\ cm^{-1}$), and a low-lying structured band located between 334 nm and 425 nm (C).

By inspection we can see that the C band seems to be constituted by a shoulder at 350 nm ($\varepsilon = 4088\ L\ mol^{-1}\ cm^{-1}$) and at least two peaks: one at 396.4 nm ($\varepsilon = 8804\ L\ mol^{-1}\ cm^{-1}$) and the other at 378.4 nm ($\varepsilon = 9870\ L\ mol^{-1}\ cm^{-1}$), respectively attributed to $S_0 \rightarrow S_1$ and $S_0 \rightarrow S_2$, with an energy gap of about 12 kJ mol^{-1} between them. The molar absorptivities at this absorption band are compatible with π,π^* transitions at the inferior limit of the range of allowed molar absorptivities [37–39]. The oscillator strengths estimated by TD-DFT calculation, for vertical transitions related to these two electronic transitions ($S_0 \rightarrow S_1$ at 381.7 nm, with $f = 0.0388$, and $S_0 \rightarrow S_2$ at 377.3 nm, with $f = 0.1092$), suggest a similar trend.

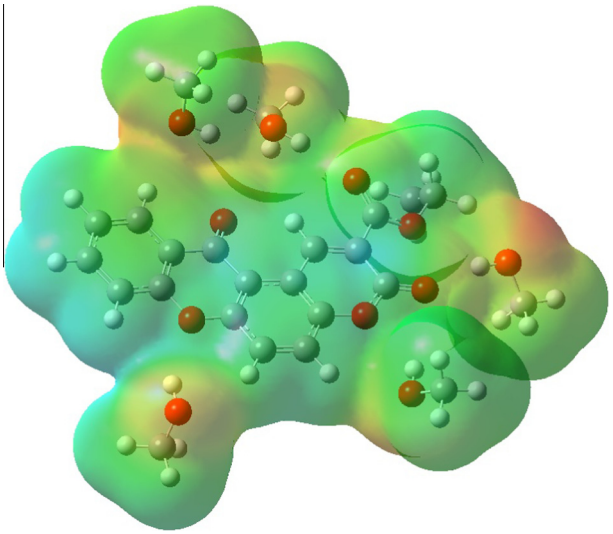

Fig. 2. Total electron density for the model employed to describe PXO1 and five explicit methanol molecules, involved by a continuum of uniform dielectric constant corresponding to methanol, generated by IEFPCM, and optimized at the CASSCF level. The 6-31G(d,p) basis set was employed in this optimization.

Gaussian deconvolution performed on the absorption spectrum suggests that at least seven sub bands participate in the electronic absorption process (solid blue curves in Fig. 3).

Table 1 summarizes the position of the maxima of the sub bands as well as their energy differences.

The energy gap between these sub bands (Table 1 and Fig. 3) shows that the bands A, B and C are formed by the overlap between close absorption sub bands assigned to different sets of electronic-vibrational transitions. In fact, the analysis of the electronic states and molecular orbitals (MOs) in the range of the TD-DFT simula-

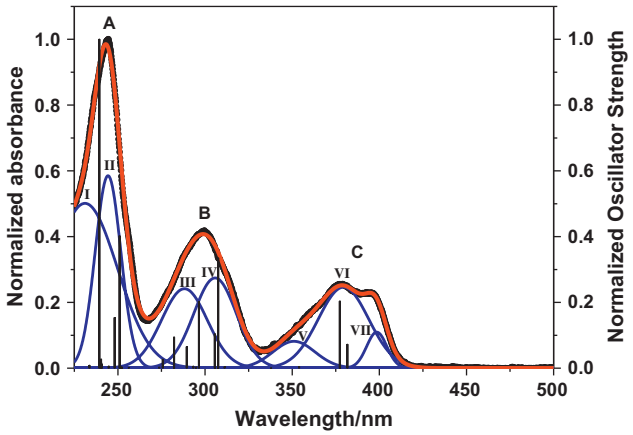

Fig. 3. Absorption spectrum for Ethyl 3,12-dioxopyran[3,2-a]xanthene-2-carboxylate (PXO1) in methanol (black solid circles). The red solid lines correspond to the simulated spectrum obtained from the deconvolution employing seven Gaussian functions (blue solid lines). The vertical lines correspond to the theoretical transitions, calculated from the optimized structure. (For interpretation of the references to colour in this figure legend, the reader is referred to the web version of this article.)

Table 1
Absorption maxima and energy difference for the deconvoluted sub bands.

Sub band	I	II	III	IV	V	VI	VII
λ (nm)	231	244	288	306	351	379	398
ΔE (kJ mol^{-1})	≈24	≈75	≈24	≈50	≈25	≈12	

tion shows four discrete transitions associated to the C-band ($S_0 \rightarrow S_1$ to $S_0 \rightarrow S_4$), eleven to B ($S_0 \rightarrow S_5$ to $S_0 \rightarrow S_{15}$), and ten to A-band ($S_0 \rightarrow S_{16}$ to $S_0 \rightarrow S_{25}$), in the simulated range of wavelengths.

The first two electronic transitions related to the C-band are of $^1(\pi,\pi^*)$ nature with a partial $^1(n,\pi^*)$ character. The energy calculated for these transitions presents a good agreement with the absorption maxima experimentally estimated (a deviation of 0.12 eV for $S_0 \rightarrow S_1$, and of 0.01 eV for $S_0 \rightarrow S_2$). Estimations of singlet-singlet transition energies using B3LYP or other hybrid functionals incorporating 15–30% of exact exchange usually give, for low-lying singlet transitions, mean signed absolute errors (MAE) in the range between 0.2 and 0.3 eV [40,41].

Still concerning the C-band, the Gaussian deconvolution confirms the number of sub-bands that compose it, the peak values (351, 379 and 398 nm) and the energy gap of about 12 kJ mol^{-1} between the low lying absorption peaks. The transition $S_0 \rightarrow S_3$, of very low probability and n,π^* character (0.0024, at 353.96 nm), is related to the sub band V (Fig. 3), responsible for the shoulder observed between the C and B-bands, which suggests the occurrence of a charge transfer process involving the solvent and the π system of PXO1.

The main differences between the calculated and experimental data regarding transitions $S_0 \rightarrow S_1$ and $S_0 \rightarrow S_2$, are associated to the ratio of intensities and the energy gap between the peak values. While the experimental intensity ratio between the least and the most energetic peak is about 0.90, the theoretical intensity ratio is equal to 0.36. The experimentally estimated energy gap between the peak values is about 12 kJ mol^{-1}, while the predicted value between S_2 and S_1 is 3.6 kJ mol^{-1} (0.0374 eV). This discrepancy may be related to the uncertainty that exists in the attribution of the calculated electronic transitions with peak values observed experimentally, which are not necessarily related to states with $v = 0$. In the first case, the difference can be attributed, at least in part to the limited number of explicit solvent molecules used to build the model used in this study. This should limit the number of electronic-vibrational states arising from solute-solvent interactions, compromising the description of changes in the spectrum more dependent on solute-solvent interactions. Although we have achieved a good description of the electronic spectrum, from the optimized "supermolecule" in comparison with other approaches used in order to obtain the most appropriate description of the electronic structure of PXO1 (not shown), we recognize that this model can be improved. It is very likely that optimized structures with an even greater level of electronic correlation combined to more complex atomic basis sets, and the inclusion of a higher number of explicit solvent molecules, could imply in an even less qualitative description of the system under study. However, the computational cost involved may not compensate the improvement achieved.

The absorption maximum at 300.0 nm, related to the B-band in the experimental absorption spectrum, of $^1(\pi,\pi^*)$ character, should have correspondence ($\Delta E = -0.10$ eV) with the transition $S_0 \rightarrow S_7$ predicted to occur by TD-DFT calculation, at 307.5 nm, with an oscillator strength ($f = 0.1794$) typical of $^1(\pi,\pi^*)$ transitions.

In the A-band, the absorption maximum at 244.0 nm has a good correspondence with the theoretical transition $S_0 \rightarrow S_{24}$ at 239.3 nm ($\Delta E = 0.10$ eV), with oscillator strength ($f = 0.5357$) also typical of $^1(\pi,\pi^*)$ transitions.

Some of the electronic transitions analyzed are also related to charge transfer processes involving oxygen non-bonding orbitals from methanol and the π system of PXO1(not shown), which highlights the importance of hydrogen bonding between PXO1 and the solvent on the spectroscopic behavior of this compound.

The electronic spectrum was also done using other atomic basis sets (6-31g(d,p), triple zeta valence plus polarization (TZVP) [42], quadruple zeta valence plus polarization (QZVP) [43], 6-311++G(2d,2p) and TZP-DKH [44]). However, the better convergence between the experimental and theoretical spectra was reached using the 6-311++G(2d,2p) basis set. Recent investigations hint that the selection of a much larger basis set would have a limited impact on the statistical values [40,45,46].

Fluorescence and phosphorescence spectra

Fig. 4 shows the excitation and emission spectrum of PXO1 at 298 K, and the emission spectrum at 77 K. The fluorescence at 298 K is very weak exhibiting this compound a very low fluorescence quantum yield even at low temperature (Table 2). Considering the structural rigidity of this compound, Φ_{IC} was considered near zero [39]. Therefore, $\Phi_{ISC} = 1 - \Phi_F = 0.97$.

From Fig. 4a, it may be noted that the fluorescence spectrum of PXO1 bear a good mirror image relationship of the $S_0 \rightarrow S_1$ absorption spectrum, suggesting an equivalent ordering of the vibrational levels for S_0 and S_1.

From Fig. 4b it is possible to observe a well-defined electronic-vibrational structure in the emission spectrum at 77 K, for both fluorescence and phosphorescence, evidencing the most likely electronic-vibrational levels. The fluorescence spectrum at 77 K

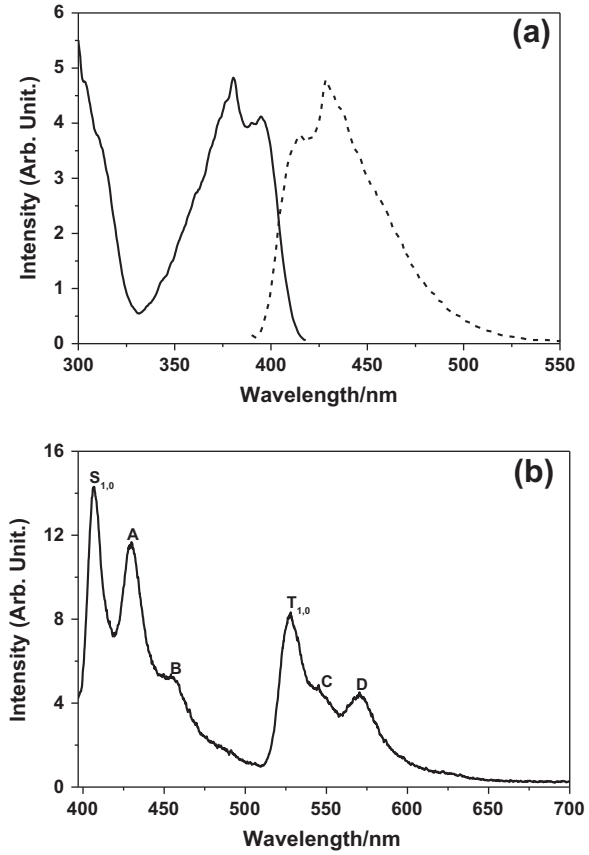

Fig. 4. (a) Excitation (black solid line) and emission (blue dashed line) spectra for PXO1 in ethanol, at 298 K. (b) Fluorescence and phosphorescence (between 520 and 650 nm) spectra at 77 K, in ethanol.

Table 2
Some photophysical data related to the compound under study.

Compound	λ_{exc}, nm	Φ_F		Φ_{ISC}	Φ_Δ
		298 K	77 K		
PXO1	379	0.00*	0.03	0.97	1.00[a,b]

* Lower than 0.001.
[a] Time-resolved measurements.
[b] Steady-state measurement.

shows three electronic-vibrational peaks ($S_{1,0}$, A and B), assigned to the decay from the bottom of the first excited singlet state to different vibrational modes of the ground state, being $S_{1,0}$, at 407 nm (24570.02 cm^{-1}), the singlet excited state that corresponds to the transition between states with $v = 0$ (Table 3). The experimental wavelength attributed to this transition is. The theoretical value estimated for this transition (428.29 nm; 23348.67 cm^{-1}) has a good agreement with the experimental (a deviation of -0.15 eV). It is necessary to highlight that the theoretical estimate of $S_{1,0}$ was done through TD-DFT calculation from previously optimized structure using CIS [34]. This approach was used for all relaxed states after unsuccessful attempts to optimize them using TD-DFT.

The phosphorescence emission spectrum can be seen in the range between 500 and 650 nm. It is noted that this spectrum also presents a well-defined electronic-vibrational structure, showing three electronic-vibrational levels ($T_{1,0}$, C and D) (Fig. 4b), assigned to the decay from the bottom of the first excited triplet state to different vibrational modes of the ground state, being $T_{1,0}$, at 528 nm (17543.86 cm^{-1}), the triplet excited state that corresponds to the transition between states with $v = 0$ (Table 3). Similar to the estimate made for $S_{1,0}$, the energy related to the wavelength theoretically estimated for $T_{1,0}$, 636.97 nm (15699.33 cm^{-1}), shows to be considerably underestimated. However, the $\Delta E = -0.40$ eV estimated between the theoretical and experimental values is in the range of MAE estimated using B3LYP (0.45 eV) for transitions involving triplet states [41,45]. For triplets, the transition energies are almost systematically underrated using TD-DFT, the average errors tending to be larger than for singlets [40].

State diagram and quantum yield of singlet oxygen generation

The state diagram obtained from TD-DFT calculations for non-relaxed singlet and triplet states of PXO1 is depicted in Fig. 5.

The expressive quantum efficiency of singlet–triplet conversion ($\Phi_{ISC} = 0.97$) expected for PXO1 (Table 2) is an evidence of an efficient population of the triplet state for this compound.

The photophysical behavior of PXO1 shows to be very similar to that observed for 3-ethoxycarbonyl-benzofuro [3,2-f] coumarin, which presents an almost unitary Φ_Δ (0.94 ± 0.06) that apparently does not depend on the characteristics of the solvent [15,16]. The structure of the electronic states of this compound, with $E(S_1) > E(T_2)$ and $\Delta E(S_2,S_1) \approx 18$ kJ mol^{-1} [16] is roughly similar to the state diagram built for PXO1, based on data from TD-DFT calculation (Fig. 5a).

The Φ_Δ estimated for PXO1 by steady-state measurements agrees very well with the value obtained by time-resolved measurements (Table 2), and suggests that the intersystem crossing

Table 3
Position of maxima and energy difference for emission bands acquired at 77 K, using anhydrous ethanol as solvent.

Band	$S_{1,0}$	A	B	$T_{1,0}$	C	D
λ (nm)	407	430	453	528	548	570
ΔE (kJ mol^{-1})	≈15.7	≈14.1	≈37.5	≈8.3	≈8.4	

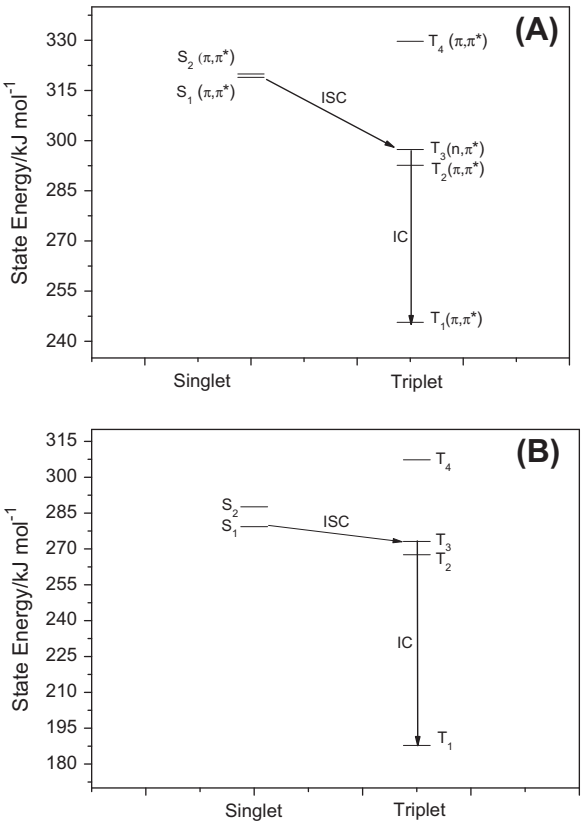

Fig. 5. Energy diagrams: (A) for non-relaxed excited states of PXO1 and (B) for the first relaxed excited states of PXO1.

should occur in very favorable conditions. Similar to the aforementioned benzopsoralens [16], the magnitude of the Φ_Δ suggests that T_1, with a triplet lifetime of 10.7 μs, is a ketonic $^3(\pi,\pi)^*$ state, confirmed by analysis of the MOs involved, which usually displays a high efficiency for singlet oxygen formation since it is usually a long-lived state [47]. In fact, our experimental data indicates to a quantum efficiency of 100% (Table 2) in both methodologies used to estimate this quantum yield, and an expressive triplet lifetime for T_1. This state is constituted by the combination of four overlapped MOs, all of $^3(\pi,\pi)^*$ nature. The prevalent are HOMO-6 → LUMO e HOMO → LUMO, this last with the greatest weight in the combination. It should be emphasized, in all of these overlaps, the participation of solvent molecules in process of charge transfer for the π system of PXO1.

In fact, the states diagram (Fig. 5a) suggests an energy gap that favors the intersystem crossing between S_1 and T_3, the adjacent triplet state. The predicted energy gap between S_1 and T_3 and between S_1 and T_1, in methanol, respectively 21.7 and 73.3 kJ mol^{-1}, is sufficiently high to compromise the reversion of the $T \rightarrow S$ conversion, warranting an efficient population of the triplet state [37–39]. Also, the different orbital symmetry of S_1 and T_3 is a good condition for an efficient $S \rightarrow T$ conversion [38,39]: while S_1 is mostly $^1(\pi,\pi^*)$, the adjacent triplet state has $^3(n,\pi^*)$ character. Thus, it suggests that the population of T_1 should occur by intersystem crossing from S_1 to T_3, followed by internal conversion from T_3 to T_1.

The triplet lifetime estimated for T_1 is consistent with the capability of sensitization of singlet oxygen production by the compound under study. The estimation of the energy to the same states, after relaxation in solvent, confirms the pattern presented, Fig. 5b, corroborating with the path proposed for the electronic population of T_1. The energy estimated for the relaxed T_1 (187.81 kJ mol^{-1}, corresponding to 636.97 nm) is also compatible for singlet oxygen sensitization, since that $E(T_1) > E(^1O_2, {}^1\Delta_g)$ [48].

Table 4
Dipole moment estimated to the relaxed excited states studied.

State	Dipole moment (D)	$\Delta\mu_{relaxed,non\text{-}relaxed}$ (D)
S_0	4.1308[a]	–
S_1	7.9261	3.7953
S_2	7.9165	3.7857
T_4	5.0419	0.9111
T_3	5.2126	1.0818
T_2	5.2135	1.0827
T_1	5.2134	1.0826

[a] The same value for each one of the non-relaxed states.

Significant conformational changes were not observed, in the electronic states surveyed, for the excited structures subsequently relaxed in solvent. On the other hand, changes in the electronic distribution, expressed in terms of Mulliken atomic charges and the changes in the dipole moment of the electronic states (Table 4), agree with the expected changes in the electronic structure of these states. A subtle rearrangement in the distribution of explicit molecules of methanol can also be observed for each of the studied relaxed electronic states.

Based on comparison of the two diagrams it is expected a decrease in the energy of the studied states as a consequence of structural relaxation in the solvent. A higher energy decrease is expected for S_1, S_2 and T_1 – this last state with a more expressive decrease, about 31%, probably due to its purest π,π^* character, followed by S_1, with about 14%. The energy gap between S_1 and S_2 tends to increase significantly (8.18 times, from 1.02 to 8.34 kJ mol^{-1}) as a result of greater relaxation of S_1, minimizing possible interferences of S_2 in the population of T_1. The minor variation of energy with the relaxation of the state in the solvent was estimated for T_3 (about 8%), due to its sharp n,π^* character. This character, as shown by the analysis of the MOs involved, is mainly due to the carbonyl group of the xanthone.

Conclusions

Summarizing, stationary as well as time resolved spectroscopic techniques in association with quantum chemical calculations were used to investigate both electronic structure and singlet oxygen production capability of a new xanthone type compound, ethyl 3,12-dioxopyran[3,2-a]xanthone-2-carboxylate (PXO1). Steady state and time resolved measurements suggest that the quantum efficiency for singlet oxygen generation is almost 100% for this compound, what qualifies it as promising candidate to be employed as phototherapeutic agent in PUVA therapy. Aiming to understand the molecular origin of so outstanding result, we investigated the electronic structure of the molecule through the use of absorption and emission spectroscopy and laser flash photolysis, correlating the experimental results with data obtained from quantum chemical calculations. A good theoretical description of the electronic spectrum was obtained, specially for states S_1 and S_2, even considering that the performed simulations were based on the B3LYP functional combined to the 6-31G(d,p) atomic basis set. The electronic spectrum was simulated by TD-DFT for PXO1 and a finite number of explicit methanol molecules under a dielectric continuum generated by IEFPCM, after previous optimization of this supermolecule using the same level of theory, shows a good agreement with the experimental one. The use of explicit solvent molecules to simulate the solute-solvent interaction show, for all electronic transitions, in addition to the electronic processes inherent to the nature of this compound, the occurrence of charge transfer from solvent to π system of PXO1, involving oxygen non-bonding orbitals from methanol, which corroborates with the low absorptivities experimentally observed for these transitions.

Finally the state diagram built from TD-DFT calculations, for singlet and triplet states, suggests an energy gap that privileges the intersystem crossing between S_1 and T_3 states. The calculated S_1–T_3 energy gap (21.77 kJ mol^{-1}) and between S_1 and T_1 (73.33 kJ mol^{-1}), in methanol, supports the high efficiency of intersystem crossing process and consequently the observed high quantum efficiency of singlet oxygen

Acknowledgements

For financial support from Fundação para a Ciência e Tecnologia, Portugal, and Brazilian research funding agencies: CNPq, INCT/INFo, FAPEMIG and CAPES. To Professors Jose Carlos N. Ferreira (Universidade Federal Rural do Rio de Janeiro) by the cession of the flash photolysis apparatus, M.S. Baptista (Universidade de São Paulo) by the cession of the singlet oxygen detection system and to Dr. D. Severino (Bioextract Farma Service, São Paulo, Brazil) for some time resolved measurements.

References

[1] F. Dall'Acqua, D. Vedaldi, S. Caffieri, in: H. Hönigsmann, G. Jori, A.R. Young (Eds.), The Fundamental Bases of Phototherapy, OEMF, Milano, 1996, pp. 1–16.
[2] V.C. Leite, R.F. Santos, L.C. Chen, L.A. Guillo, J. Photochem. Photobiol. B 76 (2004) 49–53.
[3] A. Chilin, C. Marzano, A. Guiotto, P. Manzini, F. Baccichetti, F. Carlassare, F. Bordin, J. Med. Chem. 42 (1999) 2936–2945.
[4] S.I. Ahmad, M. Yokoi, F. Hanaoka, J. Photochem. Photobiol. B 116 (2012) 30–36.
[5] F. Trautinger, Photoimmunol. Photomed. 27 (2011) 68–74.
[6] D.S. Sarnoff, R. Saini, J. Drugs Dermatol. 7 (2008) 475–478.
[7] A. Pacifico, G. Leone, Photodermatol. Photoimmunol. Photomed. 216 (2011) 261–277.
[8] S. Hayashi, M. Ikeda, Y. Kitamura, Y. Hamasaki, A. Hatamochi, J. Dermatol. Sci. 67 (2012) 20–25.
[9] A.Y. Potapenko Jr., J. Photochem. Photobiol. B 9 (1991) 1–33.
[10] R.S. Stern, N. Engl, J. Med. 357 (2007) 682–690.
[11] S. Mobilio, L. Tondelli, M. Capobianco, O. Gia, Photochem. Photobiol. 61 (1995) 113–117.
[12] M. Palumbo, P. Rodighiero, O. Gia, A. Guiotto, S.M. Magno, Photochem. Photobiol. 44 (1986) 1–4.
[13] F. Bordin, Int. J. Photoenergy 1 (1999) 1–6.
[14] C. Lage, M. Pádula, T.A.M. Alencar, S.R.F. Gonçalves, L.S. Vidal, J. Cabral-Neto, A.C. Leitão, Mutat. Res. 544 (2003) 143–157.
[15] A.M.A.G. Oliveira, M.M.M. Raposo, A.M.F. Oliveira-Campos, J. Griffiths, A.E.H. Machado, Helv. Chim. Acta 86 (2003) 2900–2907.
[16] A.E.H. Machado, J.A. Miranda, A.M.F. Oliveira-Campos, D. Severino, D.E. Nicodem, J. Photochem. Photobiol. A 146 (2001) 75–81.
[17] S. Caffieri, Photochem. Photobiol. Sci. 1 (2002) 149–157.
[18] D.E.J.G.J. Dolmans, D. Fukumura, R.K. Jain, Nat. Rev.: Cancer 3 (2003) 380–387.
[19] A.M.A.G. Oliveira, A.M.F. Oliveira Campos, M.M.M. Raposo, A.E.H. Machado, P. Puapairoj, M. Pedro, M.S.J. Nascimento, C. Portela, C. Afonso, M. Pinto, Eur. J. Med. Chem. 41 (2003) 367–372.
[20] A.J. Gomes, C.N. Lunardi, L.O. Lunardi, D.L. Pitol, A.E.H. Machado, Micron 39 (2008) 40–44.
[21] A.J. Gomes, R.M.N. Assunção, G. Rodrigues, E.M. Espreafico, A.E.H. Machado, J. Appl. Polym. Sci. 105 (2007) 964–972.
[22] A.J. Gomes, A.S. Faustino, C.N. Lunardi, L.O. Lunardi, A.E.H. Machado, Int. J. Pharm. 332 (2007) 153–160.
[23] A.J. Gomes, A.S. Faustino, A.E.H. Machado, M.E.D. Zaniquelli, T.P. Rigoletto, C.N. Lunardi, L.O. Lunardi, Drug Deliv. 13 (2006) 447–454.
[24] A.J. Gomes, C.N. Lunardi, F.H. Caetano, L.O. Lunardi, A.E.H. Machado, Microsc. Microanal. 12 (2006) 399–405.
[25] H. Satzger, B. Schmidt, C. Root, W. Zinth, B. Fierz, F. Krieger, T. Kiefhaber, P. Gilch, J. Phys. Chem. A 108 (2004) 10072–10079.
[26] A.M.A.G. Oliveira, A.M.F. Oliveira-Campos, L.M. Rodrigues, M.M.M. Raposo, A.E.H. Machado, M.S. Nascimento, N. Nazareth, M. Pinto, Chem. Biodivers. 4 (2007) 980–990.
[27] I.E. Borissevitch, J. Luminesc. 81 (1999) 219–224.
[28] D.F. Eaton, Pure Appl. Chem. 60 (1988) 1107–1114.
[29] R. Schmidt, C. Tanielian, R. Dunsbach, C. Wolff, J. Photochem. Photobiol. A 79 (1994) 11–17.
[30] R. De Paula, M.Sc. Dissertation, Universidade Federal de Uberlândia, Brazil, 2003.
[31] J. Tomasi, B. Mennucci, E. Cancès, J. Mol. Struct. (Theochem) 464 (1999) 211–226.
[32] G. Scalmani, M.J. Frisch, J. Chem. Phys. 132 (2010) 114110.
[33] a) A.D. Becke, J. Chem. Phys. 98 (1993) 5648–5652;
b) C.T. Lee, W.T. Yang, R.G. Parr, Phys. Rev. B 37 (1998) 785–789.
[34] J.B. Foresman, M. Head-Gordon, J.A. Pople, M.J. Frisch, J. Phys. Chem. 96 (1992) 135–149.

[35] M.J. Frisch, G.W. Trucks, H.B. Schlegel, G.E. Scuseria, M.A. Robb, J.R. Cheeseman, G. Scalmani, V. Barone, B. Mennucci, G.A. Petersson, H. Nakatsuji, M. Caricato, X. Li, H.P. Hratchian, A.F. Izmaylov, J. Bloino, G. Zheng, J.L. Sonnenberg, M. Hada, M. Ehara, K. Toyota, R. Fukuda, J. Hasegawa, M. Ishida, T. Nakajima, Y. Honda, O. Kitao, H. Nakai, T. Vreven, J.A. Montgomery Jr., J.E. Peralta, F. Ogliaro, M. Bearpark, J.J. Heyd, E. Brothers, K.N. Kudin, V.N. Staroverov, T. Keith, R. Kobayashi, J. Normand, K. Raghavachari, A. Rendell, J.C. Burant, S.S. Iyengar, J. Tomasi, M. Cossi, N. Rega, J.M. Millam, M. Klene, J.E. Knox, J.B. Cross, V. Bakken, C. Adamo, J. Jaramillo, R. Gomperts, R.E. Stratmann, O. Yazyev, A.J. Austin, R. Cammi, C. Pomelli, J.W. Ochterski, R.L. Martin, K. Morokuma, V.G. Zakrzewski, G.A. Voth, P. Salvador, J.J. Dannenberg, S. Dapprich, A.D. Daniels, O. Farkas, J.B. Foresman, J.V. Ortiz, J. Cioslowski, D.J. Fox, Gaussian 09, Revision C.01, Gaussian, Inc., Wallingford CT, 2010.
[36] GaussView 5.0.8. Gaussian, Inc., Wallingford, USA, 2008.
[37] D.C. Harris, M.D. Bertolucci, in: Symmetry and Spectroscopy: An Introduction to vibrational and electronic spectroscopy, Dover Publications, New York, USA, 1989.
[38] A. Gilbert, J. Baggott, in: Essentials of Molecular Photochemistry, Blackwell, London, UK, 1991.
[39] N.J. Turro, V. Ramamurthy, J.C. Scaiano, in: Modern Molecular Photochemistry of Organic Molecules, University Science Books, Sausalito, USA, 2010.
[40] D. Jacquemin, B. Mennucci, C. Adamo, Phys. Chem. Chem. Phys. 13 (2011) 16987–16998.
[41] D. Jacquemin, V. Wathelet, E.A. Perpète, C. Adamo, J. Chem. Theory Comput. 5 (2009) 2420–2435.
[42] a) A. Schaefer, H. Horn, R. Ahlrichs, J. Chem. Phys. 97 (1992) 2571–2577; b) A. Schaefer, C. Huber, R. Ahlrichs, J. Chem. Phys. 100 (1994) 5829–5835.
[43] F. Weigend, R. Ahlrichs, Phys. Chem. Chem. Phys. 7 (2005) 3297–3305.
[44] F.E. Jorge, A. Canal Neto, G.G. Camiletti, S.F. Machado, J. Chem. Phys. 130 (2009) 064108.
[45] D. Jacquemin, E.A. Perpète, I. Cifoni, C. Adamo, J. Chem. Theory Comput. 6 (2010) 1532–1537.
[46] M.R. Silva-Junior, M. Schreiber, S.P.A. Sauer, W. Thiel, J. Chem. Phys. 133 (2010) 174318.
[47] (a) R.W. Redmond, S.E. Braslavsky, Chem. Phys. Lett. 148 (1988) 523–529; (b) J. Bendig, T.R. Schmidt, H.D. Brauer, Chem. Phys. Lett. 202 (1993) 535–541; (c) W.N. Nau, J.C. Scaiano, J. Phys. Chem. 100 (1996) 11360–11367.
[48] F. Wilkinson, W.P. Helman, A.B. Ross, J. Phys. Chem. Ref. Data 24 (1995) 663–1021.